Cerebral Involvement in Stargardt's Disease: A VBM and TBSS Study

Gaia Olivo,[*,1] Paolo Melillo,[*,2] Sirio Cocozza,[1] Francesco Maria D'Alterio,[2] Anna Prinster,[3] Francesco Testa,[2] Arturo Brunetti,[1] Francesca Simonelli,[*,2] and Mario Quarantelli[*,3]

[1]Department of Advanced Biomedical Sciences, University "Federico II," Naples, Italy
[2]Multidisciplinary Department of Medical, Surgical, and Dental Sciences, Eye Clinic, Second University of Naples, Naples, Italy
[3]Institute of Biostructure and Bioimaging, National Research Council, Naples, Italy

Correspondence: Mario Quarantelli, Institute of Biostructure and Bioimaging, CNR, Via T. de Amicis 95, 80145, Naples, Italy; quarante@unina.it.

*GO, PM, FS, and MQ contributed equally to the work presented here and should therefore be regarded as equivalent authors.

Submitted: March 18, 2015
Accepted: August 4, 2015

Citation: Olivo G, Melillo P, Cocozza S, et al. Cerebral involvement in Stargardt's disease: a VBM and TBSS study. *Invest Ophthalmol Vis Sci*. 2015;56:7388–7397. DOI:10.1167/iovs.15-16899

Purpose. To assess whether and to what extent macro- and/or microstructural modifications are present in the brain of patients with selective central visual loss due to a juvenile macular degeneration, Stargardt's disease (STGD), taking advantage of the complementary information provided by voxel-based morphometry (VBM) and diffusion tensor imaging (DTI).

Methods. Eighteen patients with clinical and molecular diagnosis of STGD related to *ABCA4* mutations and 23 normally sighted volunteers of comparable age and sex were enrolled. Structural T1-weighted (T1w) volumes, for brain tissue volume assessment by segmentation, and DTI, for the investigation of diffusivity parameters via a tract-based spatial statistics (TBSS) procedure, were acquired at 3 Tesla in all subjects. All patients underwent a complete ophthalmologic examination, including best-corrected visual acuity (BCVA), biomicroscopy, ophthalmoscopy, electroretinography (ERG), microperimetry, and optical coherence tomography (OCT). Correlations between imaging data and clinical measures were tested.

Results. Stargardt's disease patients showed a significant gray matter (GM) loss bilaterally in the occipital cortices, extending into the right precuneus, and in the fronto-orbital cortices. At TBSS, significant reductions in fractional anisotropy were detected throughout large regions in the supratentorial white matter (WM), more pronounced in the posterior areas. Gray matter volume correlated directly with mean visual sensitivity in the right middle frontal and left calcarine gyri, and inversely with retinal thickness in the left supramarginal gyrus.

Conclusions. In STGD, widespread microstructural WM alterations are present, suggestive of minor fiber loss coupled with GM loss, also in cortical regions not traditionally linked to visual pathways, at least partly related to the retinal damage.

Keywords: Stargardt's disease, MRI, brain atrophy, diffusion tensor

Several studies have assessed micro- and macrostructural changes in intracerebral visual pathways in visually impaired patients, using voxel-based techniques (Tables 1, 2). These have mostly analyzed heterogeneous conditions, ranging from congenital to adult-onset pathologies, leading to somewhat conflicting results.

In particular, studies of gray matter (GM) atrophy have variously shown either selective GM loss in visual cortices[1] or the associated involvement of deep GM[2,3] or cerebral cortex.[3,4] On the other hand, results of studies of white matter (WM) integrity either were negative[5] or showed a selective involvement of visual pathways,[6–10] or more diffuse alterations in supratentorial WM.[2,11–14] This may be partly due to the inclusion of patients with blindness and/or reduced visual acuity, secondary to both congenital and acquired pathologies, comprising also tumors, infectious diseases, trauma, inherited retinal dystrophies, or retinopathy of prematurity, which at least in some cases may also affect directly the brain and/or be associated with optic nerve neuronal loss.

A more specific group of conditions leading to selective visual impairment is the macular degenerations (MDs), which include two major groups of disease, namely juvenile and age-related forms, with different etiopathogeneses.

Previous studies[1,15–18] have used voxel-based morphometry (VBM) to assess the regional volume changes of GM and WM in cohorts with mixed types of hereditary MDs,[16,18] demonstrating volumetric reductions limited to the WM of the optic pathways (including optic nerves, chiasm, the lateral geniculate bodies, and the optic radiations) and to the visual GM regions, while more extensive WM loss in frontal regions was found in age-related MD.[16]

White matter integrity has been tested only in patients with Alström syndrome (an inherited ciliopathy with early progressive cone–rod dystrophy),[15] showing a diffuse decrease in fractional anisotropy (FA), with increased radial diffusivity (RD, a parameter linked to myelin integrity). However, in this pathology these alterations are likely to be linked to the underlying ciliopathy, in view of the pivotal role of cilia in the embryogenic mechanisms leading to WM formation.

Stargardt's disease (STGD) is a juvenile hereditary MD characterized by selective gradual loss of retinal photoreceptors, leading to progressive loss of central vision, without known associated neurologic involvement.

The aim of our study was to assess whether and to what extent macro- and/or microstructural modifications were present in the brain of a group of patients with selective

Table 1. Studies of Brain Alterations in Patients With Macular Degeneration

Ref.	NV, No.	Congenital, No. (Causes)	Early, No. (Causes)	Late, No. (Causes)	DTI	Morphometry
Hernowo et al.[16]	55	–	34 (n/s)	24 (n/s)		VBM and ROI based: optic pathways and visual cortex; frontal white matter volume loss only in age-related MD
Plank et al.[18]	26	–	26 (STGD, C1D, CRD, CACD, UHMD)	–		VBM: visual cortex
Boucard et al.[1]	12	–	–	9 (n/s)		VBM: visual cortex
Manara et al.[17]	19	–	11 (CRD)	–	TBSS*: reduced FA and increased RD in OR	VBM*: visual cortex, occipital WM
Citton et al.[15]	19	–	12 (CRD)	–	TBSS: diffusely reduced FA and increased RD in supratentorial structures, increased ADC and AD in fornix	VBM: diffuse cortical atrophy, more prominent in occipital and temporal regions

Results of previous studies reporting results of voxel-based analysis of gray matter atrophy and white matter diffusion properties in patients with macular degeneration. n/s, blindness causes not specified; CD, cone dystrophy; CRD, cone–rod dystrophy; CACD, central areolar choroidal dystrophy; UHMD, unclassified hereditary macular dystrophy; ROI, retinopathy of immaturity.

* Analysis carried out only on occipital lobes/visual pathways.

central visual loss due to STGD, taking advantage of the complementary information provided by VBM and diffusion tensor imaging (DTI).

Materials and Methods

Patients

The present study conformed to the tenets of the Declaration of Helsinki and was approved by the local Institutional Review Board of the Second University of Naples. Written consent to participate in the study was obtained from all participants.

Eighteen patients (12 males, mean age 30.6 years; range, 15–54) with clinical and molecular diagnosis of STGD1 related to *ABCA4* mutations and 23 normally sighted volunteers (NV) of comparable age (mean age 30.8 years; range, 18–60) and sex (15 males) were enrolled. All subjects were right-handed. None of the subjects showed any associated systemic disease, such as neurologic pathology.

The clinical diagnosis of STGD was based on a recorded family history compatible with autosomal recessive inheritance, presence of bilateral impairment of central vision, atrophic macular lesions (a beaten-metal appearance or large patches of atrophy) with or without the appearance of perimacular and/or peripheral white-yellow flecks, and normal to subnormal electroretinogram (ERG).

Within 1 month from the magnetic resonance imaging (MRI), all patients underwent a complete ophthalmologic examination, which included the following tests: best-corrected visual acuity (BCVA) with manifested refraction by Snellen visual chart, slit-lamp biomicroscopy of anterior segment and fundus examination, full-field ERG, microperimetry, and optical coherence tomography (OCT).

Fundus lesions were classified according to Fishman et al.[19] as follows. Phenotype I included patients with small atrophic-appearing foveal lesions and localized perifoveal yellowish-white flecks; phenotype II included patients with numerous yellowish-white fundus lesions throughout the posterior pole; and phenotype III included patients with extensive atrophic-appearing changes in the retinal pigmented epithelium (RPE).

Full-field ERG was recorded by corneal contact lens electrodes with a Ganzfeld stimulator (EREV 2000 Electrophysiology system; LACE Elettronica, Pisa, Italy) according to the recommendation of the International Society for Clinical Electrophysiology of Vision (ISCEV).[20] Electroretinogram abnormalities were classified into three groups based on the following criteria proposed by Lois et al.[21]: Group I had normal full-field amplitudes; group II had normal scotopic rod ERG but reduced photopic b-wave amplitudes; and group III had ERG abnormalities involving both scotopic and photopic b-wave amplitudes.

Optical coherence tomography was performed with Cirrus HD-OCT (Carl Zeiss, Dublin, CA, USA). The acquisition protocol comprised both a five-line raster scan and a macular cube scan pattern (512 × 128 pixels) in which a 6- × 6-mm region of the retina was scanned within a scan time of 2.4 seconds. A recently developed and validated algorithm was used to quantify the area of disease in the RPE, referred to as the RPE lesion area (RPE-LA).[22] In particular, the lesion area was defined as the site presenting a significant deviation in RPE contour, an approach that proved to compare favorably with hand-drawn segmentation in terms of accuracy (Weisbrod M., et al. *IOVS* 2008;49:ARVO E-Abstract 4240), reproducibility (Gregori G, et al. *IOVS* 2007;48:ARVO E-Abstract 153), and clinical applicability.[23,24]

In addition, combined ganglion cell and inner plexiform layer thickness (GCIPL-T) was recorded.

Microperimetry (MP) was performed by an automatic fundus-related perimeter (MP1 Microperimeter; Nidek Technologies, Padova, Italy). The following parameters were used: a fixation target of 2° in diameter consisting of a red ring and a white, monochromatic background with a luminance of 1.27 cd/m^2. Retinal sensitivity was measured using a Goldman III size stimulus with intensity ranging from 0 to 20 dB and with a projection time of 200 ms; a 10-2 pattern, covering 10° centered onto PRL (preferred retinal locus) with 68 stimuli. The following MP parameters were computed: mean sensitivity (MS), dense scotoma size (DSS), the percentage of fixation points within 2° (fixation stability FS 2°) and within 4° diameter circle (fixation stability FS 4°) centered on PRL. The percentage values were used to define three grades of fixation stability: (I) stable, when more than 75% of fixations fall within the 2° circle; (II) relatively stable, when more than 75% of fixations

Table 2. Studies of Brain Alterations in Patients With Other Causes of Blindness

	NV	Congenital	Early	Late		
Ref.	No.	No. (Causes)	No. (Causes)	No. (Causes)	DTI	Morphometry
Boucard et al.[1]	12			9 (GL)		VBM: visual cortex
Bridge et al.[2]	26	6 (anophtalmia)			TBSS: (neg.) DTT: (neg.) VBA: occipital lobe, corpus callosum	VBM: visual cortex, putamen
Chen et al.[6]	24			25 (GL)	TBSS: optic tracts, ORs	
Dai et al.[7]	25			25 (GL)	VBA: optic chiasm, ORs	
Lepore et al.[4]	16		16 (LF, RB, OT, DR, LCA, ET, RP, GL)	16 (LF, RB, OT, DR, LCA, ET, RP, GL)		TBM in early onset: dorsal visual cortex, cingulate, left supplementary motor area, premotor area, superior parietal lobule TBM in late-onset: visual cortex and parietal regions
Milesi et al.[8]	25		13 (LHON)		TBSS: bilateral OR and optic tracts	
Park et al.[11]	25		18 (n/s)		VBA: visual pathway, parietal "U" fibers, striatum, pulvinar, ILF and SLF	
Ptito et al.[3]	21	11 (n/s)				VBM: dorsal lateral geniculate nucleus, right posterior pulvinar, occipital lobes, middle temporal gyri, caudate and lenticular nuclei, posterior hippocampi, fornix, right superior frontal gyrus, right inferior temporal gyrus, right lateral orbital cortex, right posterior insula
Schoth et al.[5]	11		6 (RP, CM)		DTT: (neg.)	
Shimony et al.[9]	7	5 (ROP, LCA)			DTT: CGT, iuxtacortical (V1/V2)	
Shu et al.[12]	17		17 (RP, OA, GL, LF, CC)		TBSS: CGT DTT: CGT VBA: lingual gyri, temporal-occipital regions	
Wang et al.[13]	40	20 (n/s)		21 (n/s)	TBSS: ORs (in both CB and LB), corpus callosum, anterior thalamic radiations, frontal and parietal WM (in late).Increased FA in CST (in congenital) VBA: consistent with TBSS	
Yu et al.[14]	17	14 (RP, CGL, OA, CC)	3 (CGL)		DTT: CST, OR, and posterior CC	
Zhang et al.[10]	20			20 (RP, GL, OI, ST, HF)	DTT: optic tracts	

Results of previous studies reporting results of voxel-based analysis of gray matter atrophy and white matter diffusion properties in congenital, early-, and late-onset blindness. n/s, blindness causes not specified; neg., no differences detected between patients and NV; ROP, retinopathy of prematurity; LCA, Leber's congenital amaurosis; LF, lenticular fibroplasia; RB, retinoblastoma; OT, orbit tumor; DR, detachment of the retina; ET, eye trauma; RP, retinitis pigmentosa; GL, glaucoma; LHON, Leber's hereditary optic neuropathy; CM, childhood meningitis; OA, optic nerve atrophy/hyperplasia; CC, congenital cataract; CGL, congenital glaucoma; OI, orbit infection; ST, sellar tumor; HF, high fever in teenage; DTT, diffusion tensor tractography; CGT, cortico-geniculate tractus; CB, congenital blindness; LB, late blindness; CST, corticospinal tract.

Table 3. Demographic and Genetic Data of STGD Patients

Age	Sex	*ABCR* Mutations	Age of Onset
19	F	250insCAAA G1961E D498N 4017ins24bp	11
18	M	L541P/A1038V IVS40+5g->a	14
25	M	L541P/A1038V G1961E	17
15	F	G1961E R2149X	13
48	M	N96D IVS40+5G>A	38
29	M	G1961E L1938L L1894L S1689P	25
23	F	L541P/A1038V F655C	14
33	M	R152Q G1961E 402ins24bp	18
21	M	A60V G1961E	15
23	M	G690V A1598D	11
27	M	G1961E R2149X	11
51	F	V615A G1961E	25
54	M	N96D N1436I	28
21	M	250insCAAA P402A	13
25	F	R1448K c.5018+2T>C	21
49	M	4538insC IVS40+5G>A	18
23	F	G1961E c.6282+1G>C	18
46	M	N96D N1436I	30

fall within the 4° circle; and (III) unstable, when less than 75% of fixations fall within the 4° circle.

Finally, the eccentricity and polar angle of the PRL were assessed: Eccentricity is the distance between the PRL and the fovea in degrees of visual angle; polar angle is the angle between the upward vertical axis from the fovea and a line connecting the PRL and the fovea in a clockwise direction in retinal coordinates.

Normally sighted volunteers had no history of psychiatric or neurologic disorders or treatment with medication active on the central nervous system, and had no macular abnormalities as assessed by ophthalmologic examination (i.e., slit-lamp biomicroscopy of anterior segment and fundus examination) and BCVA of 20/20 or above.

Demographic information and clinical data of patients are reported in Tables 3 and 4.

MRI Acquisition

All MRI studies were carried out at 3 Tesla on the same MRI scanner (Trio; Siemens Medical Systems, Erlangen, Germany).

Acquisition included a structural T1-weighted (T1w) volume for brain tissue volume assessment by segmentation and a DTI volume acquired within the same scanning session.

Structural T1w volumes were acquired by three-dimensional magnetization prepared rapid gradient-echo sequence (TE = 3.4 ms; TR = 1900 ms; TI = 900 ms; flip angle = 9°, FOV = 250; voxel size = 0.98 × 0.98 × 1.00 mm^3; 160 axial slices).

Diffusion tensor imaging data were acquired using an echo-planar imaging sequence (TR/TE 5200/82 ms, voxel 1.8 × 1.8 × 3.3 mm^3, 64 directions uniformly distributed in tbree-dimensional space,[25] B-factors 0 and 1000 s/mm^2, 9 B0 images equally spaced throughout the DTI acquisition, 45 axial slices covering the whole brain.

During the MRI study, the subjects lay supine with the head lightly fixed by straps and foam pads to minimize head movement.

VBM Analysis

Structural data were analyzed using a fast diffeomorphic registration algorithm (Diffeomorphic Anatomical Registration using Exponentiated Lie algebra, DARTEL[26]) and VBM,[27,28] implemented in the Statistical Parametric Mapping software package (SPM8; http://www.fil.ion.ucl.ac.uk/spm, provided in the public domain by Wellcome Trust Centre for Neuroimaging, University College London). For all the DARTEL preprocessing steps the default SPM8 parameters were used.

Briefly, the DARTEL procedure is based on a preliminary segmentation into GM and WM of the T1w volumes using the unified segmentation model as implemented in SPM8.[29] Gray matter and WM segments are then simultaneously warped to the common DARTEL space. A local GM template is then generated through an iterative nonlinear registration,[26] which is normalized to the standard anatomic space of the Montreal Neurological Institute,[30] and the resulting deformations are applied to the GM volume of each subject.

The normalized GM maps (resampled to a 1.5 × 1.5 × 1.5-mm^3 voxel size) were visually assessed to ensure good quality of the normalization.

Resulting maps were then modulated by the Jacobian determinants derived from the spatial normalization procedure, to preserve the local GM volumes, and then smoothed using an isotropic Gaussian kernel (6mm Full width at half maximum).

For each segmented T1w volume, total intracranial volume was calculated on the nonnormalized segmented volumes as the number of the voxels where the sum of GM, WM, and cerebrospinal fluid probabilities exceeded 50%.

Finally, normalized modulated GM maps were statistically analyzed using the general linear model based on the random Gaussian field theory.[31] Age and total intracranial volume were entered as nuisance regressor (confounding covariate) in an analysis of covariance to correct for age-related brain tissue volume changes and to normalize for head size. Regression analysis was carried out on voxels surviving a threshold of 10% of GM probability.

Between-group differences were probed using a threshold of $P < 0.05$, controlled for family-wise error (FWE) rate by multiple comparison correction at cluster level (following preselection of voxels surviving an uncorrected threshold of $P < 0.001$).

Tract-Based Spatial Statistics (TBSS)

All DTI datasets were preliminarily corrected for head movements and eddy current distortions using Medical Image Processing, Analysis and Visualization software (MIPAV; available in the public domain at http://mipav.cit.nih.gov). Each diffusion-weighted volume was deformed to match the corresponding nondiffusion-weighted (B0) volume using a cubic Lagrangian interpolation. Diffusion sensitizing gradient directions were corrected according to the corresponding deformation vectors,[32] and a diffusion-tensor model was fitted at each voxel using Diffusion Toolkit (available in the public domain at http://trackvis.org/dtk), generating FA, axial diffusivity (AD, the first eigenvalue of the diffusion vector), RD (average of the second and third eigenvalues of the diffusion tensor), and apparent diffusion coefficient (ADC) maps.

The TBSS analysis was performed using the FMRIB Software Library (FSL, provided in the public domain by the Oxford Centre for Functional Magnetic Resonance Imaging of the Brain).

Fractional anisotropy images of all subjects were aligned to a common target (FMRIB58_FA; available in the public domain at http://fsl.fmrib.ox.ac.uk/fsl/fsl4.0/tbss/FMRIB58_FA.html) in the MNI 152 standard space (available in the public domain at http://www.bic.mni.mcgill.ca/ServicesAtlases/ICBM152NLin6) using nonlinear registration, and interpolated to a 1 × 1 × 1–mm^3

Table 4. Clinical Data of STGD Patients

	BCVA	Fundus	MP						OCT			ERG		
Dominance	LogMAR	Fishman Score	MS	FS 2°	FS 4°	PRL Eccentricity	PRL Polar Angle	DSS	CRT	GCIPL-T	RPE-LA	Scotopic	Photopic	Lois Class
L	1/0.9	II/II	10.8/8.8	28/12	64/48	16/11	325/325	5.7/15.3	118/135	35/34	5.3/4	172.5/182.4	145.1/158.7	I/I
L	0.7/0.7	I/I	17.4/19.1	82/60	99/98	7/5	255/255	1.2/0.3	122/122	57/41	2.1/1.3	186.8/189.9	104/90.9	I/I
L	0.6/0.6	I/I	15.7/16.9	50/55	85/89	4/3	325/45	1.2/0.9	144/137	33/31	0.8/1.1	137.6/123.4	69.1/68.6	II/II
R	0.9/1	I/I	12.8/11.1	34/36	78/82	4/3	295/45	5.1/1.2	87/97	16/14	0/0	125.5/104.7	101.6/89.2	I/I
R	1/0.8	III/III	6.3/0.6	12/30	45/75	4/6	80/95	9.9/7.2	131/136	26/26	16.8/10.9	219.7/249.4	69.6/95.2	II/II
R	0.8/0.9	I/I	18.6/18.6	60/37	90/82	4/4	10/10	0.3/0.3	149/143	33/25	0/0	242.4/271.4	176.3/138.5	I/I
L	0.8/0.9	II/II	11.5/15.6	27/10	72/43	9/8	100/260	5.7/0.6	93/114	27/33	3.3/8	69.8/70.4	83.6/64.6	III/III
L	0.7/0.7	I/I	15.5/13.6	18/27	62/56	7/7	350/340	0.9/0.9	86/126	25/22	0.3/0.3	227.1/217.3	215.1/202.9	I/I
R	0.7/0.7	I/I	10.6/14.4	64/8	96/28	6/5	350/30	6/0.3	149/154	30/34	0.8/2.1	187.3/176.7	135/143.3	I/I
R	0.9/1	II/II	20/20	32/25	94/62	13/17	315/335	0/0	57/74	4/9	4.7/7.8	113.8/135.5	86.9/71.9	II/II
R	0.9/0.9	I/I	14.9/15	20/28	62/71	8/10	350/10	1.2/0.6	100/118	11/22	2.6/2.7	105/121.3	133.2/116.8	I/I
R	0.4/1	II/II	16.7/15.3	9/15	40/52	4/3	250/110	0.3/5.1	151/128	25/16	0/2	251.6/272.6	230.1/214.7	I/I
L	0.4/0	II/I	12.7/19.1	4/47	8/85	3/3	250/130	0/0	161/273	44/84	1/0	227.6/206.7	205/191.9	I/I
L	0.9/0.8	I/I	0.7/2	5/68	22/94	2/3	180/260	15.3/15.6	150/160	28/35	1.2/0.5	30.3/68.4	35.3/27.5	III/III
R	0.9/0.9	I/I	7.4/8.2	48/32	92/80	1/4	250/25	11.4/10.2	68/68	17/12	0.7/1.6	349.4/346.2	225.3/287.8	I/I
R	1/1	III/III	0/0.5	38/46	78/83	7/10	90/255	20/20	189/196	34/41	10.1/16.2	44.7/49.8	34.8/38.6	III/III
R	0.7/0.7	I/I	17.8/16.5	50/55	85/89	6/3	330/50	0.3/0	188/173	71/72	0/0	357/305	146/146	I/I
L	0.2/0	II/II	0/0	2/98	13/99	2/4	260/100	20/20	131/154	27/35	0.1/0.1	93.6/88	30.3/31.7	II/II

Right/left (R, L) eye data are reported.

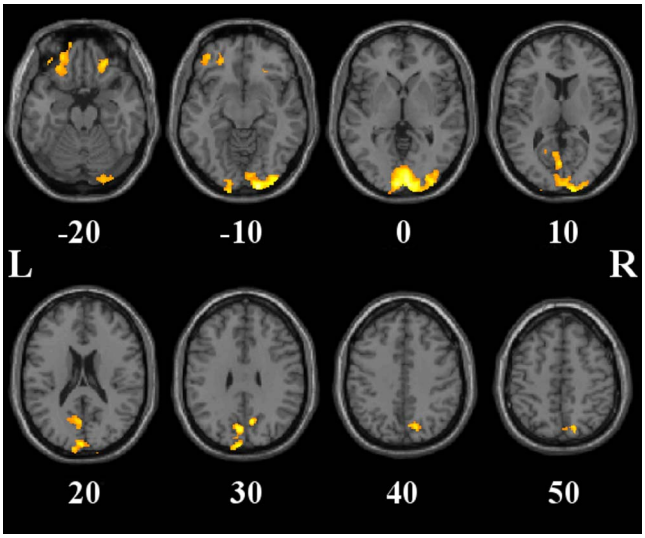

FIGURE 1. Results of the VBM analysis. Clusters of reduced GM volume in STGD patients compared to NV are superimposed on axial slices from a single subject T1-weighted volume provided by SPM8. The number of millimeters above the bicommissural plane in the MNI space is indicated for each axial section.

voxel size. Normalized FA maps were visually assessed to ensure good quality of the normalization.

For each study, the normalization parameters were then applied also to the ADC, AD, and RD maps of each subject.

Tract-based spatial statistics were then run with FA maps to create the "skeleton," which represents the center of all fiber bundles in common to all subjects,[33] using a threshold of FA > 0.3.

Each subject's aligned FA, ADC, AD, and RD data were then projected onto this skeleton, and the resulting data were fed into voxel-wise cross-subject statistics.

Nonparametric statistical analysis was done in FSL based on permutation analysis[34] applied to the general linear model (5000 permutations), including age as nuisance covariate.

Resulting statistical maps were thresholded at $P < 0.05$ corrected for multiple comparisons at a cluster level using the threshold-free cluster enhancement (TFCE) approach.[33]

Group comparisons of ADC, AD, and RD images, respectively, were also similarly performed.

Correlations Between GM Atrophy and WM Integrity

Possible correlations between the regional GM loss as detected at VBM and the FA alterations detected at TBSS were assessed separately in NV and STGD patients. To this end, for each cluster that was significantly different in STGD patients compared to NV at the VBM analysis, the corresponding mean values of the normalized modulated GM maps were measured. Clusters spanning across the two hemispheres were split into right and left subdivisions.

Similarly, for TBSS, the mean FA was measured for each of the 20 WM tracts defined in the Johns Hopkins University WM tractography atlas,[35–37] masked by the FA skeleton voxels significantly different between NV and STGD patients. Only WM tracts involved for more than 0.1 mL were considered.

Both GM volumes and FA data were then corrected for age-related changes, as measured in the NV group, by linear regression analysis. Correlations between resulting standardized residuals of GM volumes and FA data were then assessed pairwise by nonparametric correlation analysis using Spearman's coefficient, to test the relationship between GM volume in each atrophic region and FA values in abnormal WM tracts.

Correlations Between Imaging and Measures of Disease Severity

Correlation analysis was performed to assess voxel-wise possible correlations of clinical severity scores with either GM VBM or WM TBSS data, respectively.

The following clinical measures were tested for relationship with imaging data: BCVA (measured by the logarithm of the minimum angle of resolution, logMAR), Fishman class (valuated at fundus examination[19]), the ERG class defined according to Lois,[21] central retinal thickness (CRT) and GCIPL-T (measured at OCT), and MS and FS 2°, both measured at microperimetry.

Given the substantial symmetry of the pathology, right- and left-eye clinical measures were averaged for subsequent analysis, with the exception of the FS 2°, which was significantly asymmetric in most patients. For FS 2° the value of the dominant eye was used for clinical imaging correlations, in agreement with Plank et al.[18]

Voxel-based morphometry was used to assess voxel-wise the possible correlation of the selected clinical scores with the modulated normalized GM maps, including age and total intracranial volume as nuisance covariate, to identify clusters of voxels in which fractional GM volume relates to these parameters.

Tract-based spatial statistics with permutation analysis[34] were used to test possible correlations of WM microstructural integrity separately with each of the selected clinical scores, including age as nuisance covariate.

TABLE 5. VBM Results

			MNI Coordinates, mm			
	mL	T	X	Y	Z	
Cluster 1	26.0	7.39	20	−97	−6	R calcarine gyrus
		6.72	6	−93	−2	L calcarine gyrus
		6.28	−3	−76	31	L cuneus
		5.53	33	−93	1	R middle occipital gyrus
		5.19	18	−94	−15	R lingual gyrus
Cluster 2	3.0	4.24	−26	41	−11	L middle orbital gyrus
		4.07	−21	29	−23	L superior orbital gyrus
Cluster 3	2.2	6.69	12	−72	45	R precuneus
Cluster 4	1.5	4.76	26	39	−20	R middle orbital gyrus
		4.63	20	35	−17	R superior orbital gyrus
Cluster 5	1.4	4.95	−38	41	−17	L inferior frontal gyrus, pars orbitalis
		4.64	−38	47	−9	L middle orbital gyrus

Clusters showing significantly decreased gray matter volume in STGD patients ($P < 0.05$, FWE corrected at cluster level) are reported, along with the involved GM volume, the corresponding maximum T values (the equivalent of Student's t value derived from the general linear model), and coordinates in the MNI space of the local maxima. No significant differences emerged when probing the opposite (STGD > NV) contrast. Anatomic labeling is according to Ref. 52.

Table 6. Regions of Decreased FA as Detected by TBSS in STGD Patients

Structure	R	L
Posterior thalamic radiation, including optic radiation	718	71
Posterior corona radiata	396	126
Superior corona radiata	286	114
Superior longitudinal fasciculus	400	
Anterior corona radiata		201
Retrolenticular part of internal capsule	159	
Sagittal stratum, including ILF and IFOF	76	
Fornix (cres)/stria terminalis	50	
Splenium of corpus callosum	444	
Body of corpus callosum	962	

Cubic millimeters of the WM skeleton obtained as for the TBSS procedure are reported for each WM tract defined in the Johns Hopkins University WM tractography atlas.[35–37] Only structures involved for more than 50 mm^3 are reported.

Given the exploratory nature of the work, for both clinical imaging correlation analyses, results were considered significant for $P < 0.05$, corrected for multiple comparisons at cluster level based on false discovery rate (FDR).[38]

Results

Voxel-Based Morphometry

Results of VBM are shown in Figure 1 and summarized in Table 5. Stargardt's disease patients showed a significant GM loss bilaterally in the occipital cortices (with a greater extension on the right), diffusely involving calcarine gyri, and with a smaller cluster of GM loss in the adjacent parietal lobe on the right (within the precuneus). Three additional clusters of GM atrophy were found in the orbital cortices bilaterally.

No differences in GM or WM regional volumes emerged when testing the opposite contrast (STGD > NV).

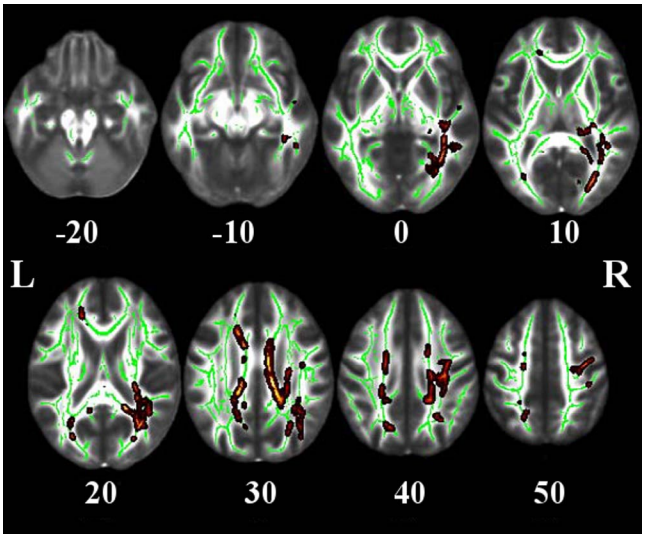

Figure 2. Results of the TBSS analysis of FA. Tracts with decreased FA in STGD patients compared to NV are reported superimposed on the mean FA map of all the subjects. The levels in the MNI space are the same as in Figure 1.

Table 7. Correlations With Clinical Data: VBM

	cc	T	MNI Coordinates, mm X	Y	Z	
CRT	6.0	9.96	−63	−24	30	L supramarginal gyrus
		7.42	−59	−13	28	L postcentral gyrus
MS	5.2	7.77	24	45	33	R middle frontal gyrus
		4.66	18	51	39	R superior frontal gyrus
	4.0	7.05	−8	−88	−5	L calcarine gyrus
		5.48	−18	−93	−17	L lingual gyrus
		4.28	−18	−75	−15	L cerebellum, VI

Clusters showing significant correlations between GM volume and disease severity ($P < 0.008$, FDR corrected at cluster level) are reported, along with the involved GM volume, the corresponding maximum T values, and coordinates in the MNI space of the local maxima. GM volume correlated directly with MS, while correlation with CRT was inverse. Anatomic labeling is according to Ref. 52.

Tract-Based Spatial Statistics

At TBSS, significant reductions in FA were detected throughout large regions in the supratentorial WM (Table 6; Fig. 2, Supplementary Fig. 1), more pronounced in the posterior areas, where several main WM bundles are located interconnecting the occipital cortices (through the splenium of the corpus callosum), as well as connecting the visual cortex to other cortical regions (optic radiations [OR]), inferior fronto-occipital fasciculus (IFOF), inferior longitudinal fasciculus (ILF), and superior longitudinal fasciculus (SLF). In addition, corona radiata was involved bilaterally along with the body of the corpus callosum. The reductions in FA were not coupled with significant increases in either ADC or axial or radial diffusivities.

When assessing regions of increased FA or of reduced diffusivity in patients, compared to NV, no significant clusters emerged. No differences between patients and NV could be detected in any of the diffusion parameters in the subtentorial structures.

Correlations Between GM Atrophy and WM Integrity

When assessing the relationship between FA in each abnormal WM tract detected at TBSS, as well as the GM volumes in the clusters of atrophy detected at VBM, no significant correlations emerged either in NV or in STGD patients.

Correlations Between Structural Imaging and Clinical Data

Results of correlation between GM volume and clinical data are reported in Table 7. Two clusters of significant direct correlation with MS (i.e., less GM volume in more severely affected patients) emerged, respectively, in the right middle frontal gyrus, extending into the adjacent superior frontal gyrus, and in the left calcarine gyrus, extending into the adjacent lingual gyrus.

In addition, a cluster of significant inverse correlation (i.e., greater local GM volume in more severely affected patients) emerged for CRT in left supramarginal gyrus, extending into the left adjacent postcentral gyrus.

No other clinical variables showed significant correlations with GM volume with the exception of GCIPL-T, which showed a cluster of inverse correlation with GM volume in the left inferior parietal lobe, partially overlapping with the

regions correlating with CRT, which, however, did not survive FDR correction for multiple comparisons.

No correlations emerged between the clinical variables and the microstructural alterations of WM tracts detected at TBSS.

Discussion

This is, to the best of our knowledge, the first study that, taking advantage of the complementary information provided by VBM and DTI, assessed both macro- (by VBM) and microstructural (by TBSS analysis of DTI) alterations over the whole brain of a group of patients with STGD.

Previous whole-brain VBM studies of GM loss in MD have detected cortical atrophy[1,16,18] essentially limited to visual cortices and visual pathways, with the exception of patients with Alström syndrome,[15,17] in whom extensive clusters of GM volume reduction were found throughout the brain, with a prevalence in the occipital cortices and in the superior temporal gyri. In addition, in this disease extensive supratentorial WM alterations were detected by TBSS analysis of DTI.

However, it should be considered that in Alström syndrome these alterations are likely to be linked to the underlying ciliopathy, in view of the pivotal role of cilia in the embryogenic mechanisms leading to brain development (extensive brain malformations are found in other ciliopathies, such as Bardet-Biedl syndrome or Joubert syndrome).

In addition, as Alström syndrome is characterized by multiorgan dysfunction, structural brain changes may be also linked to comorbidities with neurologic relevance, typical of this disease (hearing loss, obesity, type 2 diabetes mellitus, and progressive hepatic and renal failure).

In STGD we found, besides the atrophy of occipital cortices, a significant GM loss also outside of the occipital cortices, in frontobasal regions bilaterally. However, the pathogenesis and clinical significance of these alterations remain a matter of debate, as typically no neurologic involvement has been related to STGD. Indeed, the diagnosis of STGD, when MD is associated with neurologic symptoms, is considered questionable; the possible exceptions of scattered reports of neurologic impairment[39,40] have been, however, in some cases reported in association with genetic defects with significant neurologic implications (e.g., 21 trisomy). Accordingly, at least some of these alterations may be considered a consequence of visual deprivation on the visual system and on the brain regions connected to it, mediated by axonal degeneration and loss of synapses.

Indeed, in the only previous study of WM alterations in MD, reduced frontal WM volumes were demonstrated using VBM analysis of WM,[16] although only in patients with age-related pathology as opposed to the juvenile form of the disease.

The discrepancy between the results in patients with early- versus late-onset visual deprivation has been at least partially related to plasticity phenomena,[4,41,42] more represented in early-onset pathologies,[13] which may result in a partial protection against degenerative effects induced by the visual deprivation in brain regions connected to the visual cortices.

Our results using DTI and TBSS demonstrate in STGD a widespread reduction of FA in several WM structures, not limited to regions relevant to the optic pathways, although more prominently in posterior areas, where connection fibers of the occipital cortex are located, mitigating against this hypothesis.

Indeed our TBSS results only partly differ from those reported by Hernowo et al.[16] In particular, the pattern of WM volume reduction in the occipital regions of patients with juvenile MD reported in that work partly matches the involvement of optic radiations that we found. Of course the clusters in the two works do not overlap spatially. In fact, the TBSS procedure contracts in the center of the major tracts (along the so-called skeleton) the diffusion values, while the VBM procedure, which focuses on volume changes, tends to localize the differences at the periphery of the involved regions, at the interface with the other tissues. In addition, the VBM procedure has a limited sensitivity to structural alterations.[43] On the other hand, the alterations in nonoccipital WM regions that we found, which were not detected in the aforementioned paper, may very well be due, apart from the differences in patient populations, to the different sensitivities of the two techniques, as diffusion parameters reflect subtle microstructural changes, which may not directly translate into volumetric changes, being partially compensated by accompanying phenomena such as gliosis and vacuolization.[44]

Furthermore, these findings are also in agreement with previous studies in early non MD-related blindness, which have assessed microstructural alteration of WM across the whole brain by voxel-based analysis (VBA) and/or TBSS,[11,12] showing significant alterations outside the optic pathways.

Alternatively, the presence of volumetric and microstructural alterations outside of the optic pathways may still be a specific feature of the disease, as it has been found in a patient group selected with the same clinical phenotype (STGD) and proven molecular diagnosis (two *ABCA4* gene mutations), thus excluding that other comorbidities could interfere with the results.

Further studies are thus needed to clarify the mechanisms underlying these widespread WM changes detected outside of the optic pathways.

When assessing clinical imaging correlations with VBM results, we found a positive correlation between occipital GM volume and disease severity, assessed by MS, along with a frontal cluster (right superior and middle frontal gyri, close to frontal eye field) showing the same correlation pattern, possibly related to deafferentation from occipital cortices.

Interestingly, these results are consistent with the only previous study that assessed correlations of GM volume with disease severity in juvenile MD.[18]

Consistent with this hypothesis, the greater atrophy of the right occipital cortex was coupled with a preferential location of PRLs, in this patient group, in retinal portions projecting to the left occipital lobe (in 24 out of the 35 eyes where the PRL was lateralized, Table 4). This lateralization may result in a more sustained stimulation of the left visual cortex, which in turn may have provided protection against GM degeneration.

In addition, in our patients an inverse correlation between disease severity, in terms of retinal thickness, and left supramarginal gyrus, extending into the adjacent postcentral gyrus, was detected. As the inferior parietal lobe is involved, among others, in oculomotor mechanisms, specifically linked to the adaptive recalibration of eye–hand coordination,[45] a possible compensatory role can be hypothesized for this correlation, subserving adaptive oculomotor learning.

On the other hand, contrary to other studies in acquired blindness,[6,7] in our patients no significant correlations were present between structural WM alterations and disease severity, in terms of both ocular alterations and visual acuity reduction.

In addition, in the present patient group, FA decreases were not paralleled by significant diffusivity changes, a pattern that suggests the presence of a relatively minor fiber loss[46] without significant tissue loss, a condition typically associated to lowered FA with only minor increases in diffusivity,[47,48] not reaching the significance threshold. Under these conditions, limited room for detecting a significant correlation with clinical data is present.

It should also be noted here that in order to keep scan time small, to minimize patient discomfort and intrascan motion, we used nonisotropic voxels to grant coverage of the whole brain while keeping a high angular resolution (which improves stability of diffusion parameters[49,50]).

Although anisotropic voxels induce geometry-dependent changes in tract diffusion parameters,[51] these would result in voxels where crossing fibers are present, in a reduction of the differences between groups in specific WM tracts, which would in turn lead to a type II rather than type I error. Accordingly, the FA differences detected in the present analysis cannot be generated by this limitation of the current DTI acquisition protocol.

Future longitudinal studies spanning earlier and possibly asymptomatic stages of the disease should help clarify the heterogeneous pattern of correlations with clinical status. In addition, other functional tests, such as multifocal ERG, could be used to correlate regionally the retinal involvement with the cerebral structural alterations detected at MRI.

In conclusion, in STGD, widespread microstructural WM alterations are present, coupled with GM loss also in cortical regions not traditionally linked to visual pathways. Although the extent of retinal damage and the consequent severity of visual impairment seem to play a role in determining these modifications, as well in inducing plastic changes due to adaptation phenomena, other factors could influence the pattern and the severity of these alterations. Further studies in larger patient groups are needed to clarify the clinical correlates of these alterations.

Acknowledgments

Disclosure: **G. Olivo**, None; **P. Melillo**, None; **S. Cocozza**, None; **F.M. D'Alterio**, None; **A. Prinster**, None; **F. Testa**, None; **A. Brunetti**, None; **F. Simonelli**, None; **M. Quarantelli**, None

References

1. Boucard CC, Hernowo AT, Maguire RP, et al. Changes in cortical grey matter density associated with long-standing retinal visual field defects. *Brain*. 2009;132:1898–1906.
2. Bridge H, Cowey A, Ragge N, Watkins K. Imaging studies in congenital anophthalmia reveal preservation of brain architecture in "visual" cortex. *Brain*. 2009;132:3467–3480.
3. Ptito M, Schneider FC, Paulson OB, Kupers R. Alterations of the visual pathways in congenital blindness. *Exp Brain Res*. 2008;187:41–49.
4. Lepore N, Voss P, Lepore F, et al. Brain structure changes visualized in early- and late-onset blind subjects. *Neuroimage*. 2010;49:134–140.
5. Schoth F, Burgel U, Dorsch R, Reinges MH, Krings T. Diffusion tensor imaging in acquired blind humans. *Neurosci Lett*. 2006; 398:178–182.
6. Chen Z, Lin F, Wang J, et al. Diffusion tensor magnetic resonance imaging reveals visual pathway damage that correlates with clinical severity in glaucoma. *Clin Experiment Ophthalmol*. 2013;41:43–49.
7. Dai H, Yin D, Hu C, et al. Whole-brain voxel-based analysis of diffusion tensor MRI parameters in patients with primary open angle glaucoma and correlation with clinical glaucoma stage. *Neuroradiology*. 2013;55:233–243.
8. Milesi J, Rocca MA, Bianchi-Marzoli S, et al. Patterns of white matter diffusivity abnormalities in Leber's hereditary optic neuropathy: a tract-based spatial statistics study. *J Neurol*. 2012;259:1801–1807.
9. Shimony JS, Burton H, Epstein AA, McLaren DG, Sun SW, Snyder AZ. Diffusion tensor imaging reveals white matter reorganization in early blind humans. *Cereb Cortex*. 2006;16: 1653–1661.
10. Zhang Y, Wan S, Ge J, Zhang X. Diffusion tensor imaging reveals normal geniculocalcarine-tract integrity in acquired blindness. *Brain Res*. 2012;1458:34–39.
11. Park HJ, Jeong SO, Kim EY, et al. Reorganization of neural circuits in the blind on diffusion direction analysis. *Neuroreport*. 2007;18:1757–1760.
12. Shu N, Li J, Li K, Yu C, Jiang T. Abnormal diffusion of cerebral white matter in early blindness. *Hum Brain Mapp*. 2009;30: 220–227.
13. Wang D, Qin W, Liu Y, Zhang Y, Jiang T, Yu C. Altered white matter integrity in the congenital and late blind people. *Neural Plast*. 2013;2013:128236.
14. Yu C, Shu N, Li J, Qin W, Jiang T, Li K. Plasticity of the corticospinal tract in early blindness revealed by quantitative analysis of fractional anisotropy based on diffusion tensor tractography. *Neuroimage*. 2007;36:411–417.
15. Citton V, Favaro A, Bettini V, et al. Brain involvement in Alstrom syndrome. *Orphanet J Rare Dis*. 2013;8:24.
16. Hernowo AT, Prins D, Baseler HA, et al. Morphometric analyses of the visual pathways in macular degeneration. *Cortex*. 2014;56:99–110.
17. Manara R, Citton V, Maffei P, et al. Degeneration and plasticity of the optic pathway in alstrom syndrome. *AJNR Am J Neuroradiol*. 2015;36:160–165.
18. Plank T, Frolo J, Brandl-Ruhle S, et al. Gray matter alterations in visual cortex of patients with loss of central vision due to hereditary retinal dystrophies. *Neuroimage*. 2011;56:1556–1565.
19. Fishman GA, Stone EM, Grover S, Derlacki DJ, Haines HL, Hockey RR. Variation of clinical expression in patients with Stargardt dystrophy and sequence variations in the ABCR gene. *Arch Ophthalmol*. 1999;117:504–510.
20. Marmor MF, Fulton AB, Holder GE, Miyake Y, Brigell M, Bach M; ISCEV. Standard for full-field clinical electroretinography (2008 update). *Doc Ophthalmol*. 2009;118:69–77.
21. Lois N, Holder GE, Bunce C, Fitzke FW, Bird AC. Phenotypic subtypes of Stargardt macular dystrophy-fundus flavimaculatus. *Arch Ophthalmol*. 2001;119:359–369.
22. Ahlers C, Gotzinger E, Pircher M, et al. Imaging of the retinal pigment epithelium in age-related macular degeneration using polarization-sensitive optical coherence tomography. *Invest Ophthalmol Vis Sci*. 2010;51:2149–2157.
23. Kiss CG, Geitzenauer W, Simader C, Gregori G, Schmidt-Erfurth U. Evaluation of ranibizumab-induced changes in high-resolution optical coherence tomographic retinal morphology and their impact on visual function. *Invest Ophthalmol Vis Sci*. 2009;50:2376–2383.
24. Legarreta JE, Gregori G, Knighton RW, Punjabi OS, Lalwani GA, Puliafito CA. Three-dimensional spectral-domain optical coherence tomography images of the retina in the presence of epiretinal membranes. *Am J Ophthalmol*. 2008;145:1023–1030.
25. Jones DK, Horsfield MA, Simmons A. Optimal strategies for measuring diffusion in anisotropic systems by magnetic resonance imaging. *Magn Reson Med*. 1999;42:515–525.
26. Ashburner J. A fast diffeomorphic image registration algorithm. *Neuroimage*. 2007;38:95–113.
27. Ashburner J, Friston KJ. Voxel-based morphometry–the methods. *Neuroimage*. 2000;11:805–821.
28. Good CD, Johnsrude IS, Ashburner J, Henson RN, Friston KJ, Frackowiak RS. A voxel-based morphometric study of ageing in 465 normal adult human brains. *Neuroimage*. 2001;14:21–36.
29. Ashburner J, Friston KJ. Unified segmentation. *Neuroimage*. 2005;26:839–851.

30. Mazziotta J, Toga A, Evans A, et al. A probabilistic atlas and reference system for the human brain: International Consortium for Brain Mapping (ICBM). *Philos Trans R Soc Lond B Biol Sci*. 2001;356:1293–1322.
31. Friston KJ, Holmes AP, Poline JB, et al. Analysis of fMRI time-series revisited. *Neuroimage*. 1995;2:45–53.
32. Leemans A, Jones DK. The B-matrix must be rotated when correcting for subject motion in DTI data. *Magn Reson Med*. 2009;61:1336–1349.
33. Smith SM, Jenkinson M, Johansen-Berg H, et al. Tract-based spatial statistics: voxelwise analysis of multi-subject diffusion data. *Neuroimage*. 2006;31:1487–1505.
34. Bullmore ET, Suckling J, Overmeyer S, Rabe-Hesketh S, Taylor E, Brammer MJ. Global, voxel, and cluster tests, by theory and permutation, for a difference between two groups of structural MR images of the brain. *IEEE Trans Med Imaging*. 1999;18:32–42.
35. Hua K, Zhang J, Wakana S, et al. Tract probability maps in stereotaxic spaces: analyses of white matter anatomy and tract-specific quantification. *Neuroimage*. 2008;39:336–347.
36. Mori S. *MRI Atlas of Human White Matter*. 1st ed. Amsterdam, Boston: Elsevier; 2005: viii, 239.
37. Wakana S, Caprihan A, Panzenboeck MM, et al. Reproducibility of quantitative tractography methods applied to cerebral white matter. *Neuroimage*. 2007;36:630–644.
38. Benjamini Y, Hochberg Y. Controlling the false discovery rate: a practical and powerful approach to multiple testing. *J Roy Statist Soc B*. 1995;57:289–300.
39. Descartes M, Royal SA, Franklin J, et al. A new syndrome with Stargardt macular degeneration, abnormalities of the corpus callosum, mental retardation, and dysmorphic features: a case report of two siblings. *Clin Dysmorphol*. 2009;18:178–180.
40. Kalfakis N, Grivas I, Panayiotidou E, Sfagos C, Papageorgiou C. Stargardt's disease with neurological involvement: case report. *Funct Neurol*. 1994;9:97–100.
41. Voss P, Lassonde M, Gougoux F, Fortin M, Guillemot JP, Lepore F. Early- and late-onset blind individuals show supra-normal auditory abilities in far-space. *Curr Biol*. 2004;14:1734–1738.
42. Wittenberg GF, Werhahn KJ, Wassermann EM, Herscovitch P, Cohen LG. Functional connectivity between somatosensory and visual cortex in early blind humans. *Eur J Neurosci*. 2004;20:1923–1927.
43. Zhang L, Dean D, Liu JZ, Sahgal V, Wang X, Yue GH. Quantifying degeneration of white matter in normal aging using fractal dimension. *Neurobiol Aging*. 2007;28:1543–1555.
44. Johansen-Berg H, Behrens TEJ. *Diffusion MRI: From Quantitative Measurement to In-Vivo Neuroanatomy*. London: Academic Press; 2009;158–170.
45. Clower DM, West RA, Lynch JC, Strick PL. The inferior parietal lobule is the target of output from the superior colliculus, hippocampus, and cerebellum. *J Neurosci*. 2001;21:6283–6291.
46. Burzynska AZ, Preuschhof C, Backman L, et al. Age-related differences in white matter microstructure: region-specific patterns of diffusivity. *Neuroimage*. 2010;49:2104–2112.
47. Rovaris M, Gass A, Bammer R, et al. Diffusion MRI in multiple sclerosis. *Neurology*. 2005;65:1526–1532.
48. Sen PN, Basser PJ. A model for diffusion in white matter in the brain. *Biophys J*. 2005;89:2927–2938.
49. Zhu T, Liu X, Gaugh MD, et al. Evaluation of measurement uncertainties in human diffusion tensor imaging (DTI)-derived parameters and optimization of clinical DTI protocols with a wild bootstrap analysis. *J Magn Reson Imaging*. 2009;29:422–435.
50. Zhan L, Leow AD, Jahanshad N, et al. How does angular resolution affect diffusion imaging measures? *Neuroimage*. 2010;49:1357–1371.
51. Oouchi H, Yamada K, Sakai K, et al. Diffusion anisotropy measurement of brain white matter is affected by voxel size: underestimation occurs in areas with crossing fibers. *AJNR Am J Neuroradiol*. 2007;28:1102–1106.
52. Tzourio-Mazoyer N, Landeau B, Papathanassiou D, et al. Automated anatomical labeling of activations in SPM using a macroscopic anatomical parcellation of the MNI MRI single-subject brain. *Neuroimage*. 2002;15:273–289.

Investigative Ophthalmology & Visual Science